Advanced Powder Technology 35 (2024) 104395

Contents lists available at ScienceDirect

Advanced Powder Technology

journal homepage: www.elsevier.com/locate/apt

# Porosity and phase composition effects on SHS-NiTi structure and mechanical properties

Gulsharat A. Baigonakova [a], Ekaterina S. Marchenko [a], Oibek Mamazakirov [a], Alex A. Volinsky [a,b,*]

[a] Laboratory of Superelastic Biointerfaces, National Research Tomsk State University, 36, Lenin Ave., Tomsk 634050, Russia
[b] Department of Mechanical Engineering, University of South Florida, 4202 E. Fowler Ave. ENG030, Tampa, FL 33620, USA

ARTICLE INFO

*Article history:*
Received 6 October 2023
Received in revised form 18 February 2024
Accepted 5 March 2024

*Keywords:*
Porous NiTi
SHS
Implants
Porosity
Macrostructure
Mechanical properties

ABSTRACT

NiTi samples with 59–70% porosity were obtained by the self-propagating high-temperature synthesis (SHS) using Ti, Ni, and NiTi powders as inert. The maximum and average pore sizes increase, while the maximum and average dimensions of the bridges decrease with porosity, controlled by adjusting the amount of inert additives, based on the surface and cross-sectional microscopy studies. The phase composition of porous NiTi was determined by X-ray diffraction. The alloy contains an austenitic B2 TiNi phase, a martensitic B19′ TiNi phase, and a secondary $Ti_2Ni$ phase. SHS-NiTi samples with different porosity were tested by uniaxial compression, revealing mechanical properties' dependence on porosity. It is shown that with an 11% increase in the NiTi alloy porosity, the yield and compressive strength are reduced by almost a factor of 2.

Published by Elsevier B.V. on behalf of Society of Powder Technology Japan.

## 1. Introduction

NiTi-based biomaterials are widely used to restore the lost structure and functions of human bones. There is a growing demand for new and improved orthopedic implants due to a large number of needed joint replacements. In particular, there is a need for porous NiTi implants with high mechanical characteristics corresponding to those of bone tissues [1–3]. Depending on the processing conditions of porous NiTi-based materials, their porosity, the distribution of pores and interpore bridges, and their sizes can significantly affect mechanical properties, such as strength, hardness, plasticity, fatigue characteristics, Young's modulus, and superelastic properties [4–12].

The shape of the pores and porosity had a great influence on the stress–strain characteristics of porous alloys, where the critical stresses and the mechanical hysteresis area decreased with porosity [13]. The effects of pore size on the phase composition, compressive strength, elastic modulus, superelasticity, and corrosion resistance were studied at the same ~50 % porosity of NiTi alloys [12,14]. It was demonstrated that with an increase in the pore size from 98 μm to 294 μm, the amounts of secondary $Ti_2Ni$ and $TiNi_3$ phases increased, while the amount of the TiNi matrix phase decreased. The hardness, compressive strength, and elastic modulus of porous NiTi alloys tend to change with the pore size. An increase in the pore size adversely affected the corrosion resistance of porous NiTi alloys in the Hanks solution. Porous NiTi with an isotropic pore structure has a higher compressive strength compared to porous NiTi shape memory alloys (SMA) with an anisotropic pore structure, similar 53 % porosity and 200–500 μm pore size [15,16].

The effects of porosity on the mechanical and wear-resistant characteristics of NiTi alloys obtained by vacuum sintering were studied in [6]. The authors addressed the effects of voids on the wear resistance, hardness, and superelasticity of the NiTi matrix. A large number of pores adversely affected the wear resistance of the composites, so the authors improved the wear resistance by reducing the pore density using wax. The orientation of the combustion channels also affects the strength of the porous NiTi obtained by the self-propagating high-temperature synthesis (SHS) [7]. It has been established that the compressive strength increases when the pore channels are parallel to the sample compression direction and decreases when the combustion channels are perpendicular to the sample compression direction.

Monolithic NiTi has typical stress–strain curves with a martensitic stress plateau and superelastic deformation at room temperature [8–11]. However, porous NiTi with 28–45 % porosity shows almost linear elasticity. The absence of a martensitic stress plateau is due to the stress concentration around pores of various sizes. The local stress in some micro-regions around small pores can reach

* Corresponding author.
*E-mail address:* volinsky@usf.edu (A.A. Volinsky).

https://doi.org/10.1016/j.apt.2024.104395
0921-8831/Published by Elsevier B.V. on behalf of Society of Powder Technology Japan.

the critical stress of martensitic transformation even if the remotely applied nominal stress is small. Therefore, stress-induced martensite continuously appears in different micro-regions around pores of different sizes as the applied stress increases.

We studied the surface structure, corrosion and biocompatibility properties of porous NiTi alloys obtained by the SHS. However, in order to achieve good biomedical performance of NiTi implants, the porosity and the resulting mechanical properties must be taken into account. The purpose of this work is to study the effects of the pore space macrostructure and the phase composition of NiTi on the mechanical properties, controlled by the processing conditions.

## 2. Materials and methods

During the production process, it is important to obtain a uniform porous alloy structure with a certain pore size distribution. One of the problems at the powder billet preparation stage is the stratification of the charge, which subsequently leads to additional stratification of the porous alloy and an increased pore size. It is possible to reduce the stratification of the charge and porosity without changing the morphology of the powders by introducing inert frame-forming additives with a developed surface into the composition. NiTi powder with an average 50–100 μm particle size was used as inert additives up to 30 vol%. The presence of particles with a developed surface in the charge leads to the formation of large inert clusters that prevent the movement of titanium and nickel particles, covering them with stably formed cells. It is necessary to determine the optimal ratio of the average particle size of the inert additive and the volume fraction of the additive in the mixture, since its presence greatly reduces the degree of exothermicity of the mixture. Reducing the exothermicity of the mixture below the critical level leads to the termination of the exothermic reaction. In addition, violation of the optimal inert amount leads to the isolation of titanium and nickel particles and stops the reaction. Adjusting the inert amount changes the porosity: the more NiTi powder inert, the lower the porosity due to the low exothermicity of the charge (lower SHS temperature) [17]. Thus, depending on the amount of added inert NiTi powder (0–10 %), NiTi alloys with 59–70 % porosity were obtained, listed in Table 1.

Porous NiTi alloys were obtained by SHS using Ti PTOM and Ni PNK-1L5 powders, and NiTi powder as an inert (Table 2). The powders were dried in vacuum at 60–70 °C for 6 h and mixed in a V-shaped mixer for 8 h. The powder mixture was poured into quartz tubes with an inner diameter of 40 mm and compacted to a 60–70 % porosity, achieving a uniform density and uniform distribution of the powders over the entire volume of the workpiece. Then, the quartz tube with the charge was placed in the reactor and heated to 480–520 °C in a tubular electric furnace with flowing Ar for 20 min. Synthesis was initiated at the open end of the powder preform using a heated tungsten ignition coil in Fig. 1(a). Synthesis propagated is shown schematically in Fig. 1(b). After completion of the synthesis, the reactor with the resulting alloy was cooled in water while continuing to pass a flowing protective gas.

Metallographic sections were prepared according to the standard procedure. The surface of the sections was observed using an Axiovert-40 MAT optical microscope. The surfaces of the pore walls and the microstructure of the alloys were studied by scanning electron microscopy using an Axia ChemiSEM microscope (SEM, Thermo Fisher Scientific, USA). X-ray diffraction (XRD) phase analysis was performed using a Haoyuan DX-2700BH multipurpose X-ray diffractometer. The phases were identified using a PDF 4+ database with full profile analysis software POWDER CELL 2.4.

The porosity of the samples, P, was determined by weighing and using the NiTi compact density:

$$P = \left(1 - \frac{\rho_{por}}{\rho_{mon}}\right) \times 100\% \quad (1)$$

Here, $\rho_{por}$ is the density of the porous sample or powder blank, and $\rho_{mon}$ is the density of compact NiTi 6.45 g/cm$^3$. The average size of the pores and walls of the NiTi porous framework was determined by the random secant method using the ImageJ software [18–20]. Representative 10–20 optical images were selected for this purpose and random secants were constructed on each of the images. The values of the pore/pore wall sizes were determined based on the intersection of the secants. Size distribution histograms were constructed for pores and walls of the porous framework.

Sixteen samples with 59–70 % porosity in the form of 6 × 3 × 3 mm$^3$ prisms were cut out by electrical discharge machining. Compressive testing of porous samples was carried out using an Instron 3386 universal testing machine with a compression rate of 0.005 $sec^{-1}$.

**Table 1**
NiTi alloy porosity dependence on the addition of inert NiTi powder.

| Addition of inert NiTi powder | Porosity, P |
|---|---|
| 0 % | 70 % |
| 5 % | 65 % |
| 10 % | 59 % |

## 3. Results and discussion

The macrostructure of the pore space of NiTi obtained by the SHS with different additions of the inert NiTi additive (0 %, 5 %, 10 %) was studied in Fig. 2. The quantitative characteristics of the NiTi porous framework were determined and histograms of the distribution of pores and interpore walls were constructed by analyzing the optical microscopy images. The samples obtained with different additions of NiTi inert had different porosity values, and with an increase in inert amount, the porosity decreased. The sample without the addition of inert had a porosity of 70 %, and with an increase in the NiTi inert addition to 10 %, the porosity decreased to 59 %.

The size distribution of pores and walls of SHS-NiTi porous frameworks is unimodal and log normal, which is typical for finely porous samples in Fig. 3. The maximum sizes of the frame walls and pores of the 59 % porosity NiTi sample are 928 μm and 803 μm, respectively in Fig. 3(a) and (c). With an increase in porosity to 70 %, a decrease in the maximum size of the framework walls to 404 μm and an increase in the maximum pore sizes to 1,201 μm are observed in Fig. 3(b) and (d). An increase in the pore size and a decrease in the size of the bridges were also observed when the porosity changed from 59 % to 70 %. The 59 % porosity sample had an average pore wall size of 215 μm and an average pore size of 187 μm, while the 70 % porosity sample had 140 μm and 229 μm, respectively. A decrease in the pore size and porosity with the inert amount is explained by a decrease in the charge exothermicity when NiTi powder is added as an inert. At the same time, the thermal contribution of the exothermic reaction to the coalescence process is insufficient in the structuring zone of the SHS process [21,22].

X-ray diffraction spectra were obtained from porous NiTi samples in Fig. 4. It has been established that all alloys are in a mixed structural state and consist mainly of the TiNi phase in two crystallographic modifications: B2 austenite and B19′ martensite. In addition to the main diffraction lines, reflections from the $Ti_2Ni$ intermetallic phase were found in the spectra. Porous NiTi SMA

**Table 2**
Chemical composition in wt.% and size of PTOM, PNK-1L5, and TiNi powders.

| | | | | | | | |
|---|---|---|---|---|---|---|---|
| PTOM | Ti (main) | N 0.2 % | C 0.05 % | H 0.4 % | Fe + Ni 0.4 % | Si 1 % | 60–80 μm |
| PNK-1L5 | Ni (main) | C 0.28 % | Fe 0.002 % | Co/Zn/Cu 0.003 % | Cd/Sn/Sb 0.003 % | Si 0.001 % | <20 μm |
| TiNi | Ni (main) | Ti 44.9 % | Ca 0.28 % | Fe 0.11 % | C 0.4 % | – | 100–140 μm |

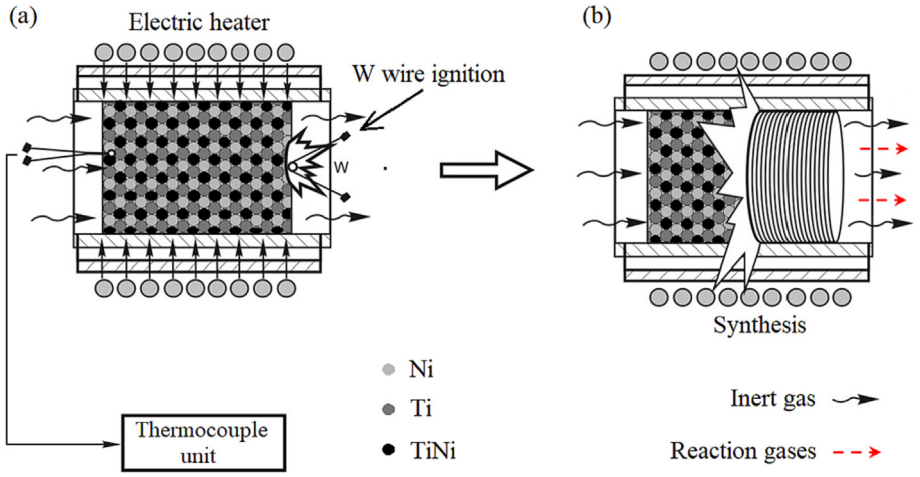


**Fig. 1.** Schematics of obtaining porous NiTi alloys by the SHS method in an open reactor with the addition of an inert: (a) synthesis start by W wire ignition and (b) synthesis propagation.

**Table 3**
Quantitative characteristics of the NiTi (B2), NiTi (B19′), and $Ti_2Ni$ phases.

| P, % | NiTi (B2), vol.% | NiTi (B19′), vol.% | $Ti_2Ni$, vol.% |
|---|---|---|---|
| 59 | 44.4 | 22.2 | 33.4 |
| 65 | 51.8 | 21.5 | 26.7 |
| 70 | 61.2 | 21.8 | 17 |

was fabricated by different researchers using SHS [23–25] and metal injection molding [26]. The same phases were identified by the XRD results in our study. It was also reported that the amount of the B2 phase increases, while the content of the $Ti_2Ni$ phase decreases with preheating temperature [23–27], which is consistent with results in Table 3.

Usually, the $Ti_2Ni$ phase is always present in the material, while $TiNi_3$, Ni, and Ti are rarely found in porous NiTi alloys produced by the SHS method. These phases were not observed in this work in Fig. 4 and Table 3. The presence of pure Ni is toxic to living tissues, and a large proportion of $Ti_2Ni$, $TiNi_3$, and $Ti_3Ni_4$ phases in porous SHS-NiTi increases the brittleness of products [28].

Scanning electron microscopy was used to study the matrix microstructure of the obtained samples. Fig. 5 shows micrographs of the NiTi alloys with different inert additives. It has been established that in all cases, two-phase dendritic regions of peritectic crystallization were formed during synthesis, consisting of light gray TiNi regions and an intergranular interlayer of a dark gray $Ti_2Ni$ phase surrounding them. There is a difference in the volume fraction of the intergranular dark gray $Ti_2Ni$ phase and TiNi regions in porous alloys. Changes in the proportion of the secondary $Ti_2Ni$ phase are associated with various additives of the inert, as well as the temperature distribution and the amount of the reaction heat in the reactor. An increase in the addition of inert leads to a decrease in the exothermicity of the mixture and, as a consequence, a decrease in porosity and an increase in the proportion of the secondary $Ti_2Ni$ phase.

Fig. 6 shows the loading-unloading superelasticity stress–strain curves of the SHS-NiTi alloys with 59 %, 65 %, and 70 % porosity. Before compression all samples are in the austenitic state with a cubic B2 lattice. The elastic regions differ slightly from the viscoelastic regions, with no martensitic stress plateau. The samples with 59–70 % porosity show 1.9–3.3 % of the recoverable strain

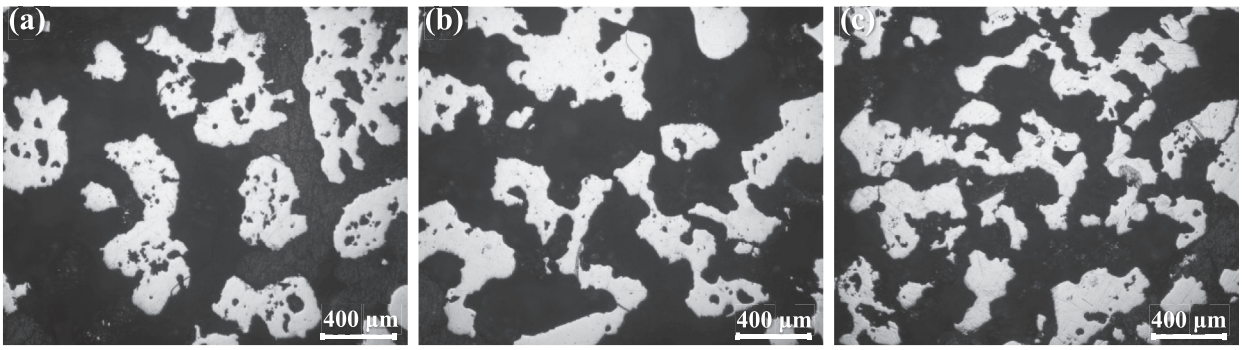


**Fig. 2.** Macrostructure of the pore space of SHS-NiTi with (a) 59%, (b) 65% and (c) 70% porosity. Here, dark regions correspond to pores, and bright regions to interpore bridges.

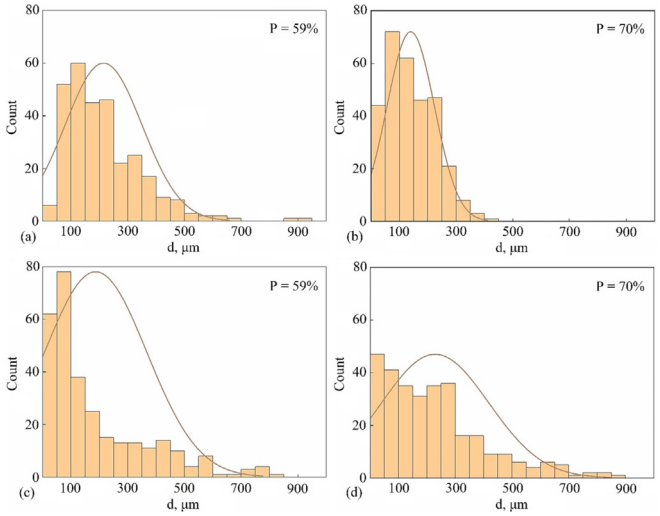


**Fig. 3.** Size distribution histograms of (a, b) framework walls and (c, d) pores in SHS-NiTi samples.

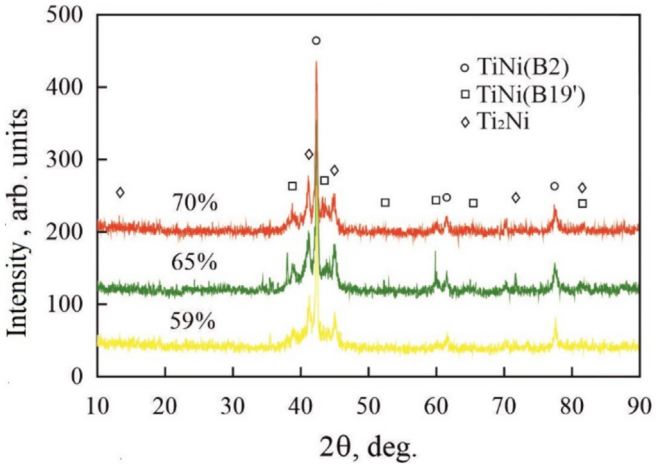


**Fig. 4.** X-ray diffraction patterns of porous SHS-NiTi alloys with different porosity.

$\varepsilon_r$ upon unloading. These results are consistent with the data of other authors [1,6,7,10].

Mechanical properties of porous NiTi with different porosity were studied by uniaxial compression to failure. Fig. 7 shows the stress–strain compression curves of the NiTi samples to failure. The compression tests showed that as the porosity increased, the mechanical characteristics of the material deteriorated. An 11 % change in porosity led to a significant reduction of the yield strength and compressive strength by almost a factor of 2 in

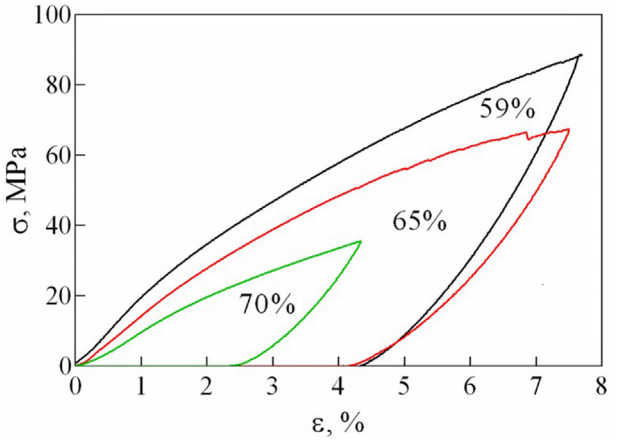


**Fig. 6.** Loading-unloading compression stress–strain curves of porous SHS-NiTi samples with different porosity.

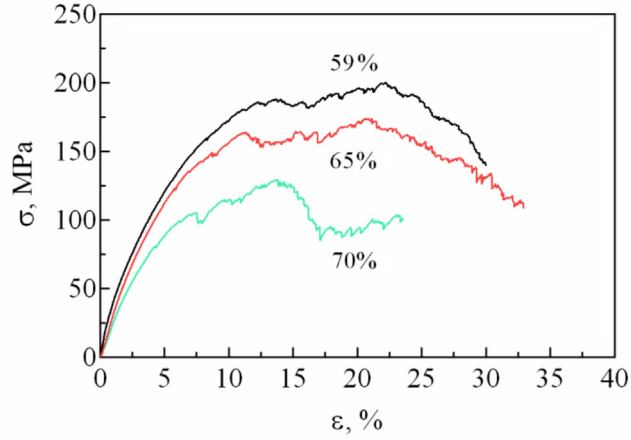


**Fig. 7.** Compression stress–strain curves to failure of porous SHS-NiTi samples with different porosity.

Table 4. With an increase in porosity from 59 % to 70 %, the compressive strength decreased from 199 MPa to 129 MPa, and the yield strength decreased from 34.47 MPa to 14.33 MPa in Table 4. In addition, an increase in the porosity of the NiTi samples to 70 % led to a decrease in the effective elastic modulus by 0.73 GPa. Apparently, the mechanical characteristics of the alloys decrease with porosity due to a decrease in the strength of the interpore bridges, as well as the stress concentrations around the pores, which are determined by their size, shape, and orientation. The frame walls decrease in size and the pore size increases up to

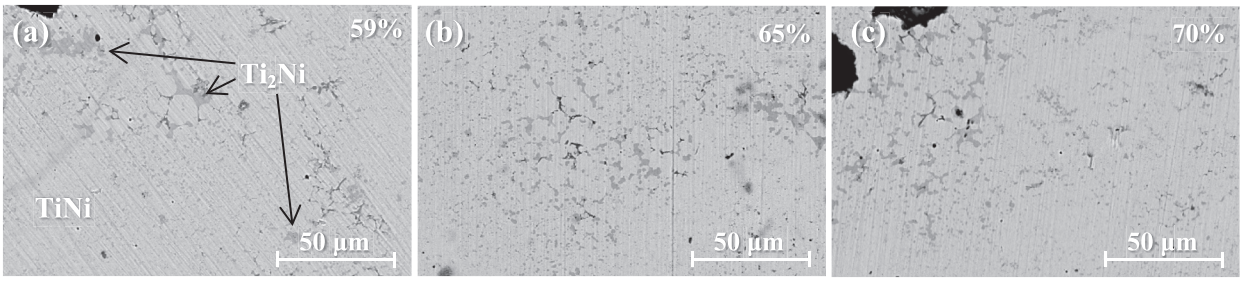


**Fig. 5.** SEM images of the SHS-NiTi with: (a) 59%, (b) 65%, and (c) 70% porosity.

**Table 4**
Mechanical characteristics of NiTi with different porosity.

| P, % | $\sigma_y$, MPa | E, GPa | $\sigma_U$, MPa | $\varepsilon_r$, % |
|---|---|---|---|---|
| 59 | 34.47 | 2.78 | 199 | 3.35 |
| 65 | 17.07 | 2.57 | 174 | 3.25 |
| 70 | 14.33 | 2.05 | 129 | 1.90 |

**Table 5**
Physical and mechanical properties of human bones [21–34].

| Properties | Cortical bone | Cancellous bones |
|---|---|---|
| Porosity, P | 5–30 % | 30–90 % |
| Pore size | 10–500 μm | 50–300 μm |
| Compressive strength | 131–224 MPa (longitudinal)<br>106–133 MPa (transverse) | 2–5 MPa |
| Elastic modulus | 17–20 GPa (longitudinal)<br>6–13 GPa (transverse) | 0.76–4 GPa |
| Reversible deformation | 2–2.5 MPa | |

1,201 μm with porosity, reducing the wall frame strength. According to the authors of [29], the maximum level of stress during fracture will be achieved when the interpore bridges are close in size. With a homogeneous macrostructure of the material and the same size of interpore bridges, the applied stress is evenly distributed over all monolithic bridges and the entire material is deformed as a whole, significantly increasing the strength. In the case of an inhomogeneous structure, when both small and massive bridges are present in the material, the sources of cracks are bridges that cannot withstand a certain level of strain under isostatic loading conditions [30]. When the load increases, they will fracture first. The redistribution of stresses leads to additional loading of non-fractured bridges.

To compare the mechanical properties of bone tissues and porous NiTi, consider Tables 4 and 5.

As seen from Table 5, the mechanical parameters of hard tissues vary in different parts of the human body. Thus, implant materials are expected to have appropriate properties to cover these differences. Strength (compressive, tensile, bending, etc.), fatigue strength and wear resistance should be taken into account first. For example, the compressive strength of bone substitute materials should be in the 131–224 MPa range [31]. The response of the implants to cyclic loads or deformations is mainly determined by the fatigue resistance of the material, which determines the long-term success of implants subjected to cyclic loads. In addition, low wear resistance can also lead to implant loosening and wear, which can cause adverse allergic reactions and shortened implant life. Second, implanted materials are expected to have a relatively low effective modulus of elasticity close to that of hard tissues (0.76–5 GPa) [32–34], since high modulus of implants can cause osteoporosis in the bone around implants due to the "stress screening effect" according to the Wolff's law, which indicates that as the load on the bone decreases, the bone adapts and becomes weaker. Third, the mechanical behavior of bone tissues must match the implants to avoid bone fractures. Some human bone tissues also exhibit behavior similar to superelasticity, and the recoverable strain can be as high as 2.5 % [35]. Thus, hard tissue replacement materials should have a similar or higher recoverable strain (>2.5 %) at body temperature.

## 4. Conclusions

NiTi samples with 59–70 % porosity were obtained by the SHS method using Ti and Ni powders, and NiTi powder as an inert. The study of the surface of thin sections and the analysis of their micrographs showed that with an increase in porosity, by adjusting the amount of inert additives, the maximum and average pore sizes increase, and the maximum and average dimensions of the frame walls decrease. The phase composition of porous NiTi was determined by XRD. The alloy contains an austenitic B2 NiTi phase, a martensitic B19′ NiTi phase, and a secondary $Ti_2Ni$ phase. As the amount of inert NiTi additive increases, the proportion of the secondary phase increases due to a decrease in the charge exothermicity. Uniaxial compression tests of SHS-NiTi with different porosity were carried out, revealing the dependence of mechanical properties on porosity. It has been established that the mechanical properties are sensitive to changes in the porosity of the material. It is shown that with an increase in the porosity by 11 %, the yield strength and ultimate strength decrease by almost 2 times. At the same time, the obtained samples demonstrate good superelasticity (1.9–3.35 % of reversible deformation), similar to human bone tissues. The mechanical characteristics of NiTi alloys deteriorate with porosity due to a decrease in the strength of interparticle contacts, as well as stress concentrations arising around pores, which are determined by their size, shape, and orientation. The obtained data on the mechanical properties of porous NiTi allow stating that they satisfy the conditions of biomechanical compatibility.

## CRediT authorship contribution statement

**Gulsharat A. Baigonakova:** Writing – original draft, Investigation, Formal analysis. **Ekaterina S. Marchenko:** Data curation, Investigation, Supervision, Resources, Project administration. **Oibek Mamazakirov:** Writing – original draft, Visualization, Validation, Methodology. **Alex A. Volinsky:** Writing – review & editing, Visualisation, Formal analysis, Project administration.

## Declaration of competing interest

The authors declare that they have no known competing financial interests or personal relationships that could have appeared to influence the work reported in this paper.

## Acknowledgments

The study was supported by the Russian Science Foundation grant No. 22-72-10037, https://rscf.ru/project/22-72-10037/.

## References

[1] Y.F. Yasenchuk, E.S. Marchenko, V.E. Gunter, A. Radkevich, O.V. Kokorev, S.V. Gunther, G.A. Baigonakova, V.N. Hodorenko, Biocompatibility and clinical application of porous NiTi alloys made by self-propagating high-temperature synthesis (SHS), Materials 12 (15) (2019) 2405, https://doi.org/10.3390/ma12152405.
[2] V.E. Gunter, Y.F. Yasenchuk, S.V. Gunther, E.S. Marchenko, M. Yuzhakov, Biocompatibility of porous SHS-TiNi, Mater. Sci. Forum 970 (2019) 320–337, https://doi.org/10.4028/www.scientific.net/MSF.970.320.
[3] S. Thomas, A. Behera, T.A. Nguyen, Nickel-titanium smart hybrid materials, in: From Micro- to Nano-structured Alloys for Emerging Applications, Elsevier, 2022, pp. 105–122.
[4] J. Ryhanen, M. Kallioinen, J. Tuukkanen, J. Junila, E. Niemela, P. Sandvik, W. Serlo, In vivo biocompatibility evaluation of nickel–titanium shape memory metal alloy: muscle and perineural tissue responses and encapsule membrane thickness, J. Biomed. Mater. Res. 41 (1998) 481–488, 0.1002/(SICI)1097–4636(19980905)41:3<481::AID-JBM19>3.0.CO;2-L.
[5] W. Tang, Q. Shen, X. Yao, W. Li, J. Jiang, Z.h. Ba, Y. Li, X. Shi, Effect of grain size on the microstructure and mechanical anisotropy of stress-induced martensitic NiTi alloys, Mater. Sci. Eng. A 849 (2022), https://doi.org/10.1016/j.msea.2022.143497 143497.
[6] H.Z. Ye, D.Y. Li, R.L. Eadie, Influences of porosity on mechanical and wear performance of pseudoelastic TiNi-matrix composites, J. Mater. Eng. Perform. 10 (2001) 178–185, https://doi.org/10.1361/105994901770345196.
[7] K.H. Mehmet, O. Nuri, T. Gül, The effect of the combustion channels on the compressive strength of porous NiTi shape memory alloy fabricated by SHS as implant material, Curr. Opin. Solid State Mater. Sci. 14 (1) (2010) 21–25, https://doi.org/10.1016/j.cossms.2009.07.002.

[8] B. Yuan, M. Zhu, C.Y. Chung, Biomedical porous shape memory alloys for hard-tissue replacement materials, Materials (basel). 11 (9) (2018) 1716, https://doi.org/10.3390/ma11091716.
[9] G. Chen, K.D. Liss, P. Cao, In situ observation and neutron diffraction of NiTi powder sintering, Acta Mater. 67 (2014) 32–44, https://doi.org/10.1016/j.actamat.2013.12.013.
[10] Z.Q. Guo, H.X. Xie, F.L. Dai, H.C. Qiang, L.J. Rong, P.W. Chen, F.L. Huang, Compressive behavior of 64% porosity NiTi alloy: An experimental study, Mater. Sci. Eng. A 515 (2009) 117–130, https://doi.org/10.1016/j.msea.2009.03.083.
[11] M. Panico, L.C. Brinson, Computational modeling of porous shape memory alloys, Int. J. Solids Struct. 45 (2008) 5613–5626, https://doi.org/10.1016/j.ijsolstr.2008.06.005.
[12] J.L. Xu, L.Z. Bao, A.H. Liu, X.F. Jin, J.M. Luo, Z.C. Zhong, Y.F. Zheng, Effect of pore sizes on the microstructure and properties of the biomedical porous NiTi alloys prepared by microwave sintering, J. Alloy. Compd. 645 (2015) 137–142, https://doi.org/10.1016/j.jallcom.2015.05.006.
[13] B. Liu, Y. Pan, Effect of pore shape on mechanical properties of porous shape memory alloy, Micromachines 13 (2022) 566, https://doi.org/10.3390/mi13040566.
[14] X.T. Sun, Z.X. Kang, X.L. Zhang, H.J. Jiang, R.F. Guan, X.P. Zhang, A comparative study on the corrosion behavior of porous and dense NiTi shape memory alloys in NaCl solution, Electrochim. Acta 56 (2011) 6389–6396, https://doi.org/10.1016/j.electacta.2011.05.019.
[15] C.Y. Chung, C.L. Chu, S.D. Wang, Porous NiTi shape memory alloy with high strength fabricated by self-propagating high-temperature synthesis, Mater. Lett. 58 (11) (2004) 1683–1686, https://doi.org/10.1016/j.matlet.2003.10.045.
[16] Y.H. Li, L.J. Rong, Y.Y. Li, Compressive property of porous NiTi alloy synthesized by combustion synthesis, J. Alloy. Compd. 345 (1,2) (2002) 271–274, https://doi.org/10.1016/S0925-8388(02)00412-7.
[17] K. Otsuka, X. Ren, Physical metallurgy of Ti–Ni-based shape memory alloys, Prog. Mater Sci. 50 (2005) 511–678, https://doi.org/10.1016/j.pmatsci.2004.10.001.
[18] W.F. Gale, T.C. Totemeier, 10 – Metallography, in: Smithells Metals Reference Book (Eds.), Butterworth-Heinemann, Oxford, 2004.
[19] A.-P.-O. Carlos, D.M.S. Jorge, Method for grain size determination in carbon steels based on the ultimate opening, Measurement 133 (2019) 193–207, https://doi.org/10.1016/j.measurement.2018.09.068.
[20] A. Lawley, T.F. Murphy, Metallography of powder metallurgy materials, Mater. Charact. 51 (5) (2003) 315–327, https://doi.org/10.1016/j.matchar.2004.01.006.
[21] V.E. Gunter, Y.F. Yasenchuk, T.L. Chekalkin, E.S. Marchenko, et al., Formation of pores and amorphous-nanocrystalline phases in porous TiNi alloys made by self-propagating high-temperature synthesis (SHS), Adv. Powder Technol. 30 (2) (2019) 1–8, https://doi.org/10.1016/j.apt.2018.12.011.
[22] Y. Yasenchuk, V. Gunther, E. Marchenko, T. Chekalkin, G. Baigonakova, V. Hodorenko, S. Gunther, J.H. Kang, S. Weiss, A. Obrosov, Formation of mineral phases in self-propagating high-temperature synthesis (SHS) of porous TiNi alloy, Mater. Res. Express 6 (5) (2019), https://doi.org/10.1088/2053-1591/ab01a1 056522.
[23] B.Y. Tay, C.W. Goh, Y.W. Gu, C.S. Lim, M.S. Yong, M.K. Ho, M.H. Myint, Porous NiTi fabricated by self-propagating high-temperature synthesis of elemental powders, J. Mater. Process. Technol. 202 (2008) 359–364, https://doi.org/10.1016/j.jmatprotec.2007.09.037.
[24] B.Y. Li, L.J. Rong, Y.Y. Li, V.E. Gjunter, Synthesis of porous Ni-Ti shape-memory alloys by self-propagating high-temperature synthesis: reaction mechanism and anisotropy in pore structure, Acta Mater. 48 (2000) 3895–3904, https://doi.org/10.1016/S1359-6454(00)00184-1.
[25] C.L. Chu, C.Y. Chung, P.H. Lin, S.D. Wang, Fabrication of porous NiTi shape memory alloy for hard tissue implants by combustion synthesis, Mater. Sci. Eng. A 366 (2004) 114–119, https://doi.org/10.1016/j.msea.2003.08.118.
[26] H. Guoxin, Z. Lixiang, F. Yunliang, L. Yanhong, J. Mater. Process. Technol. 206 (2008) 395–399.
[27] C.L. Chu, C.Y. Chung, P.H. Lin, S.D. Wang, Fabrication and properties of porous NiTi shape memory alloys for heavy load-bearing medical applications, J. Mater. Process. Technol. 169 (2005) 103–107, https://doi.org/10.1016/j.jmatprotec.2005.03.002.
[28] P. Sevilla, C. Aparicio, J.A. Planell, F.J. Gil, Comparison of the mechanical properties between tantalum and nickel-titanium foams implant materials for bone ingrowth applications, J. Alloys Comp. 439 (2007) 67–73, https://doi.org/10.1016/j.jallcom.2006.08.069.
[29] A. Bansiddhi, T.D. Sargeant, S.I. Stupp, D.C. Dunand, Porous NiTi for bone implants: a review, Acta Biomater. 4 (2008) 773–782, https://doi.org/10.1016/j.actbio.2008.02.009.
[30] A. Bandyopadhyay, I. Mitra, S.B. Goodman, M. Kumar, S. Bose, Improving biocompatibility for next generation of metallic implants, Prog. Mater. Sci. 133 (2022), https://doi.org/10.1016/j.pmatsci.2022.101053 101053.
[31] J.K. Gong, J.S. Arnold, S.H. Cohn, Composition of trabecular and cortical bone, Anat. Rec. 149 (1964) 325–331, https://doi.org/10.1002/ar.1091490303.
[32] A.W. Miles, S. Gheduzzi, Basic biomechanics and biomaterials, Surgery (Oxford) 30 (2012) 86–91, https://doi.org/10.1016/j.mpsur.2011.11.004.
[33] A. Nouri, P.D. Hodgson, C.E. Wen, Biomimetic porous titanium scaffolds for orthopedic and dental applications, in: A. Mukherjee (Ed.), Biomimetics Learning from Nature InTech, Rijek, 2010.
[34] X.J. Wang, Y.C. Li, P.D. Hodgson, C.E. Wen, Nano- and macro-scale characterization of the mechanical properties of bovine bone, Mater. Forum 31 (156–159) (2007), 10536/DRO/DU:30007337.
[35] N.B. Morgan, Medical shape memory applications–The market and its product, Mater. Sci. Eng. A 378 (2004) 16–23, https://doi.org/10.1590/S0100-879X2003000600001.